First-principles investigation of strain effects on the stacking fault energies, dislocation core structure, and Peierls stress of magnesium and its alloys

S. H. Zhang, I. J. Beyerlein, D. Legut, Z. H. Fu, Z. Zhang, S. L. Shang, Z. K. Liu, T. C. Germann, and R. F. Zhang

First principles investigations of strain effects on the stacking fault energies, dislocation core structure and Peierls stress of magnesium and its alloys

S.H. Zhang[1, 2], I.J. Beyerlein[3], D. Legut[4], Z.H. Fu[1, 2], Z. Zhang[1, 2], S.L. Shang[5], Z.K. Liu[5], T.C. Germann[6], and R.F. Zhang[1, 2,]*

[1]School of Materials Science and Engineering, Beihang University, Beijing 100191, P. R. China

[2]Center for Integrated Computational Engineering, International Research Institute for Multidisciplinary Science, Beihang University, Beijing 100191, P. R. China

[3]University of California at Santa Barbara, Santa Barbara, CA 93106, USA

[4]IT4Innovations Center, VSB-Technical University of Ostrava, CZ-70833 Ostrava, Czech Republic.

[5]Department of Materials Science and Engineering, The Pennsylvania State University, University Park, PA 16802, USA.

[6]Theoretical Division, Los Alamos National Laboratory, Los Alamos, NM, 87545, USA

* Corresponding author: zrf@buaa.edu.cn (R.F. Zhang)

ABSTRACT

Taking pure Mg, Mg-Al and Mg-Zn as prototypes, the effects of strain on the stacking fault energies (SFEs), dislocation core structure and Peierls stress were systematically investigated by means of density-functional theory and the semidiscrete variational Peierls-Nabarro model. Our results suggest that volumetric strain may significantly influence the values of SFEs of both pure Mg and its alloys, which will eventually modify the dislocation core structure, Peierls stress and preferred slip system, in agreement with recent experimental results. The so-called "strain factor" that was previously proposed for the solute strengthening could be justified as a major contribution to the strain effect on SFEs. Based on multivariate regression analysis, we proposed universal exponential relationships between the dislocation core structure, the Peierls stress and the stable or unstable SFEs. Electronic structure calculations suggest that the variations of these critical parameters controlling strength and ductility under strain can be attributed to the strain-induced electronic polarization and redistribution of valence charge density at hollow sites. These findings provide a fundamental basis for tuning the strain effect to design novel Mg alloys with both high strength and ductility.

I. INTRODUCTION

Magnesium (Mg-based) alloys are attractive for extensive automobile [1], aerospace [2,3] and biomedical applications [4] due to their high strength-to-weight ratio, low density and biodegradability [4]. However, the trade-off dilemma between strength and ductility and the poor workability and formability are two longstanding bottlenecks for the development of novel Mg alloys. It is generally believed that the strong crystallographic anisotropy and the lack of slip systems of hexagonal close packed (hcp) Mg alloys [5] are the main reasons for the poor plasticity and ductility which identify the workability and formability, while the low slip resistance to dislocation movement leads to the low strength.

Solution strengthening of Mg alloys is generally used in practice and has been well investigated by many research groups [6-11]. Its ability to enhance the energy barrier of dislocation movement without profound loss of ductility can be explained by the fact that the number of slip systems is not changed by alloying particular elements [12]. By introducing solutes, the slip resistance in the basal (0001) plane can be effectively increased, while simultaneously the critical stress for cross-slip from the basal plane to the secondary prismatic $(10\bar{1}0)$ planes is decreased. For example, Al and Zn are two typical solute elements which are experimentally found to lower the critical stress for cross slip [13].

In ductilizing Mg alloys, slip in both basal and non-basal planes must be active (as governed by the von-Mises criterion [14]) to achieve appreciable ductility. However, the stress required to plastically deform Mg alloys along its (easy) basal slip plane is two orders of magnitude lower than that of (hard) non-basal plane. To solve this problem, recent theoretical investigations suggest that the addition of effective solutes (e.g. the rare earth

elements may play a role to randomize the texture [15]) may distinctly modify the energy of I_1 type stacking fault, and thus promote the heterogeneous nucleation of pyramidal $\langle c+a \rangle$ dislocations, which will in turn benefit the ductility of Mg alloys [16]. Usually, the major role of the added different solutes is to activate more than five independent slip systems for an appreciable ductilization. The solute effect on the dislocation core structure and Peierls stress has been recently systematically studied by Pei *et al*. [17] and Yasi *et al*. [18] in order to underline the slip mechanism controlling the ductility. These studies have shown that different elements may indeed influence the slip behavior, cross slip and dislocation reaction.

Although the introduction of an appropriate solute provides an effective pathway for strengthening and ductilizing Mg alloys [12,13,19-22], the strain effects must also be included to account for the strength and ductility of Mg alloys. At equilibrium, a pure geometrical analysis indicates that the plasticity should be accommodated by the slip along five independent slip systems activated in ascending order (*i.e.*, the easiest slip system in Mg is basal slip along $\{0001\}\langle \bar{1}2\bar{1}0 \rangle$, followed by prismatic slip along $\{10\bar{1}0\}\langle \bar{1}2\bar{1}0 \rangle$, and the next easy slip systems are pyramidal plane type I along $\{10\bar{1}1\}\langle \bar{1}2\bar{1}0 \rangle$ and $\{10\bar{1}1\}\langle \bar{1}\bar{1}23 \rangle$, as well as type II along $\{11\bar{2}2\}\langle \bar{1}\bar{1}23 \rangle$ [23].) due to their different critical resolved shear stresses for slip. Under sufficient strain, however, the plastic deformation of Mg alloys cannot be simply quantified by this geometrical analysis at equilibrium because the strain will not only change the *c/a* ratio but also modify the SFEs, and eventually induce different dislocation core structures, dislocation mobilities, and the preferred slip systems. Because all these intrinsic parameters are critical in governing the plastic deformation, their variations by strains will eventually modify the mechanical strength and ductility of Mg alloys. For example, a higher

value of SFE will hinder the formation of a wider dislocation core, as a result decrease the mobility of dislocation during the loading. Recent experiments have confirmed that (a) the non-basal slip systems of Mg alloys can be activated by hydrostatic pressure [24-26]; (b) under c-axis compression the operative modes for pure Mg are $\langle c+a \rangle$ slip on pyramidal II and significant ductilizing and hardening occur [27]; and (c) compressive pre-deformation changes the deformation behavior and yield strength of a Mg-Al-Zn alloy under tensile loadings [28]. These results suggest a necessity to investigate the effect of strain on the SFEs, dislocation core structure and associated Peierls stress, which are critical in strengthening and ductilizing Mg alloys.

In the present study, we take the volumetric strain as a representative case to present the strain effect with a wide range of strain (*i.e.* $-0.12 < \Delta V/V < 0.13$, corresponding to the pressure value with -5.7~3.4 GPa) to meets not only the normal loading conditions with low strain or stress, such as less than the tensile yield strength of pure Mg, but also those special cases, under which Mg alloys can support a larger strain or stress (e.g. several GPa), such as shock loading with high strain rate, high hydrostatic pressure within confined volume and in nanocrystalline state with restricted dislocation mobilities. For example, under one-dimensional shock loading with a velocity about 500m/s, some Mg alloys can be longitudinally stressed to about 3GPa [29,30], and the effect of high pressure on the mechanical properties of Mg alloys have been studied experimentally, with a maximum pressure of 6GPa [31,32]. In section 2, we shall first describe the method of first-principles calculation, the approach to calculate the SFEs, the semidiscrete variational PN model used for the determination of dislocation core structure and the calculation details of Peierls stress.

Afterwards, the calculated results are presented in section 3: the effect of volumetric strain on the SFEs is given in subsection 3.1, and the dislocation core structure and Peierls stress in subsection 3.2. To underline the physical origin of the strain effect, an in-depth analysis of electronic structure is given in subsection 3.3. Afterwards, a discussion on the strengthening and ductilizing mechanism in Mg alloys is given in section 4. We conclude in section 5 with a recap of the major conclusions drawn in this study.

II. COMPUTATIONAL APPROACH

A. First-principles calculation

Our first-principles DFT calculations were performed using the Vienna *ab initio* simulation package (VASP) code [33] by the projector augmented wave (PAW) method [34] with the Perdew-Burke-Ernzerhof (PBE) version [35] of the Generalized Gradient Approximation (GGA) as the exchange-correlation functional. An energy cutoff of 500eV and $15 \times 15 \times 3$ *k*-mesh gamma-centered grids were used. The SFE was tested carefully for the convergence as a function of the *k*-mesh grid (see Fig. S1 in the Supplemental Material [36]). The energy convergence criterion of the electronic self-consistency is chosen as 10^{-6} eV/cell, while the force convergence criterion of ionic relaxation is used, with all forces acting on the atoms being lower than 0.01eV/Å. The Methfessel-Paxton (MP) method [37] was used for the electronic self-consistency of both ionic relaxation and energy calculation with a smearing width of 0.01 eV.

Table 1 lists the optimized lattice constants of pure Mg, which are in very good agreement with previously published experimental [38] and theoretical [39] data. The

calculated cohesive energy of pure Mg also agrees well with the results of previous theory [40], providing a further validation of the PAW pseudopotentials used for Mg alloys.

B. Stacking fault energy

The SFE describes the energy variation when two parts of a crystal are rigidly shifted with different fault vectors lying in a given crystallographic plane [41]; it is defined as:

$$\gamma = \frac{E_{SF} - E_0}{A}, \tag{1}$$

where E_{SF} and E_0 are the energies of the structure with a stacking fault and the perfect structure, respectively, and A is the area of the stacking fault plane. To calculate the SFEs, we built a periodic supercell containing 48 atoms (4 atoms/layer). The lattice vectors of the supercell are parallel to the $[11\bar{2}0]$, $[10\bar{1}0]$ and $[0001]$ directions, respectively. For Mg alloys, a Mg atom at one faulted plane (0001) was replaced by one solute atom X (X=Zn or Al). Therefore, the global solute concentration is about 2.08%, which corresponds to an areal concentration of 25% at the faulted plane for an $Mg_{47}X$ alloy. In general, there are two approaches to calculate the SFEs by means of DFT, namely alias shear [42] and slab shear [43]. The former one can be complemented by an alias shear deformation of a periodic supercell via the Cartesian coordinate representations of atomic position, while the latter one requires only the movement of atomic positions within two slabs, but requires a supercell surrounded by a sufficiently thick vacuum to eliminate any surface effects. In our study, the alias shear approach was employed for the following considerations: 1) the number of supercell atoms is only one-half of that using the slab shear technique; and 2) the stress can be directly derived from the stress-strain relationship of the simulated supercell. Fig. 1a

illustrates the configuration of an I_2 stacking fault (…ABABCACA…) that was generated from the perfect hcp structure by displacing the upper half of the supercell by $1/3[10\bar{1}0]$ while holding the bottom half fixed. The twin fault T_2 (…ABABCBABA...) can be obtained by displacing another layer of I_2 as indicated by the dotted line in Fig. 1a. In order to get the entire γ-surface, including unstable SFEs, only vertical movement normal to the slip plane was permitted during atomic relaxation.

In the present work, we firstly applied a series of volumetric strains on the supercell to study the variations of SFEs under strain. It should be noted that the volumetric strain is imposed by changing the lattice constants of *a* and *c*. During this procedure only the atomic positions were allowed to relax, with the constraint of crystallographic symmetry, and the SFEs were calculated employing the alias shear approach based on the relaxed strained supercell.

C. Dislocation core structure and Peierls stress

Three approaches are generally used to determine the dislocation core structure based on first-principles calculation: a solution based on flexible boundary conditions [44-46], an analytical solution based on dislocation dipole array [41,47], and the semidiscrete variational PN model evolved from the classic one by Bulatov *et al*. [48,49]. With the last one as our basis, the model assumption is that one dislocation line is parallel to the z-axis ($[10\bar{1}0]$) with Burgers vector $\bar{b}=1/3[11\bar{2}0]$ (x-axis), with slip on the x-z plane. The trial displacements for the edge and screw components of the partial dislocations are expressed by Eq. (2) and used to determine the equilibrium configuration of the dislocation in pure Mg and Mg alloys [50]:

$$u_x(x) = \frac{b}{2\pi}\left(\arctan\frac{x-d_x/2}{w_x} + \arctan\frac{x+d_x/2}{w_x}\right) + \frac{b}{2}$$

$$u_z(x) = \frac{\sqrt{3}b}{6\pi}\left(\arctan\frac{x-d_z/2}{w_z} - \arctan\frac{x+d_z/2}{w_z}\right)$$

(2)

where d_x (or d_z) is the separation between edge (or screw) components of the two partial dislocations, and w_x (or w_z) gives the half-width of edge (or screw) components of the two partial dislocations. An illustration of the meaning of these qualities is shown in Fig. 2. Equivalently, the dislocation core structure is described by the misfit density $\rho(x) \equiv du(x)/dx$, and the typical profiles of $u_x(x)$, $u_z(x)$, $\rho_x(x)$ and $\rho_z(x)$ are shown in Fig. 2. The γ-surface was expanded in a 2-D Fourier series as suggested in Ref. [51]:

$$
\begin{aligned}
\gamma(u_x,u_z) = {}& c_0 + c_1[\cos(2qu_z) + \cos(pu_x + qu_z) + \cos(-pu_x + qu_z)] \\
& + c_2[\cos(2pu_x) + \cos(pu_x + 3qu_z) + \cos(-pu_x + 3qu_z)] \\
& + c_3[\cos(4qu_z) + \cos(2pu_x + 2qu_z) + \cos(pu_x - 2qu_z)] \\
& + c_4\begin{bmatrix} \cos(3pu_x + qu_z) + \cos(3pu_x - qu_z) + \cos(2pu_x + 4qu_z) \\ + \cos(2pu_x - 4qu_z) + \cos(pu_x + 5qu_z) + \cos(-pu_x + 5qu_z) \end{bmatrix} \\
& + a_1[\sin(pu_x - qu_z) - \sin(pu_x + qu_z) + \sin(2qu_z)] \\
& + a_2[\sin(2pu_x - 2qu_z) - \sin(2pu_x + 2qu_z) + \sin(4qu_z)]
\end{aligned}
$$

(3)

where $p = 2\pi/b$, $q = 2\pi/(\sqrt{3}b)$ and $c_0 = -3\cdot(c_1 + c_2 + c_3 + 2c_4)$ which could be determined by applying the condition: γ(0,0)=0. The unknown coefficients c_1, c_2, c_3, c_4, a_1 and a_2 were determined by fitting the γ-surface (as illustrated in Fig. 1b) with Eq. (3) and nonlinear least square method based on Trust-Region algorithm.

The total energy of a dislocation E_{tot} is expressed as the sum of the misfit energy E_{mit} and the elastic energy E_{el} [48]:

$$E_{tot} = \sum_i \gamma(u_x(x_i), u_z(x_i))\cdot\Delta x + K_e\cdot\sum_{ij}\chi_{ij}\rho_{x,i}\rho_{x,i} + K_s\cdot\sum_{ij}\chi_{ij}\rho_{z,i}\rho_{z,i},$$

(4)

$$\rho_{x,i} = (u_{x,i} - u_{x,i-1})/(x_i - x_{i-1}), \quad \rho_{z,i} = (u_{z,i} - u_{z,i-1})/(x_i - x_{i-1}),$$

(4a)

$$\chi_{ij} = 3/2 \cdot \varphi_{i,i-1} \varphi_{j,j-1} + \psi_{i-1,j-1} + \psi_{i,j} - \psi_{i-1,j} - \psi_{i,j-1} \, , \tag{4b}$$

$$\psi_{i,j} = 1/2 \cdot \varphi_{i,j}^2 \ln |\varphi_{i,j}| \, , \quad \varphi_{i,j} = x_i - x_j \, , \tag{4c}$$

$$K_e = G/(4\pi(1-v)) \, , \quad K_s = G/(4\pi) \tag{4d}$$

where x_i are the reference positions, Δx is the average spacing of the atomic rows in the lattice,

G is the shear modulus and v is the Poisson ratio. In our calculations, a same set of elastic

constants (*i.e.* K_e=2.238 and K_s=1.647 (see Table 2 together with the experimental data [52]

and other predictions from the literature [40])) was used to determine the dislocation core

structure and Peierls stress of Mg and Mg alloys. Then, the equilibrium core structure of

dislocation defined by the parameter u_x, u_z, w_x and w_z in Eq. (2) was obtained by minimizing

the total energy E_{tot} [53], and accordingly the particle swarm optimization (PSO) algorithm

[54,55] was employed for the energy minimization in the present study.

The Peierls stress is defined as the critical resolved shear stress required to move a

dislocation across a crystal lattice [56,57]. To determine the Peierls stress, the method

proposed in Ref. [56] was employed in the present study and the misfit energy in Eq. (4) is

rewritten as

$$E_{mit}(\mu) = \sum_m \gamma \big(u_x (m\Delta x - \mu), u_z (m\Delta x - \mu) \big) \cdot \Delta x \, . \tag{5}$$

Accordingly, the Peierls stress τ_p is determined by

$$\tau_p = \max\{\tau\} = \max\left\{ \frac{1}{b} \frac{dE_{mit}(\mu)}{\mu} \right\} . \tag{6}$$

III. RESULTS

We first determined the SFEs of the unstrained Mg and its alloys, both to serve as a

baseline for validation of present studies and to understand the origin of the large scatter of

the SFEs reported in previous publications. Table 3 shows our calculated values of stable

SFEs (γ_{I_2}, γ_{T_2}) and unstable SFEs (γ_{UI_2}, γ_{UT_2}) of pure Mg and its alloys, compared with

previous calculated literature values [6-12,17,40,58-61]. For the stable SFE γ_{I_2} of pure Mg,

the experimental values vary from 50mJ/m^2 to 280mJ/m^2 [8], mostly owing to the uncertainty

in experiments such as the conditions, methods, sample purity and assumptions in the

analysis. Although most theoretical SFEs lie between 20.1-48.2mJ/m^2 for pure Mg (see Table

3), a large scatter still exists relative to the precision of DFT total energies, which are

generally within ±1meV/atom. Therefore, we have checked the convergence in the

calculation of SFEs with respect to the variations of the density of the k-point mesh grids and

different choices of cutoff energy, both of which are critical for high-precision energy

calculations. By a careful comparison, we found that the difference of the calculated SFEs in

past studies was mostly due to their different k-mesh grid points, as a lower k-mesh grid will

generate a larger scatter in the calculated SFEs (see Fig. S1 in Supplemental Materials [36]).

Given these considerations, we used a relatively high density of k-mesh grids (15×15×3) and

a high cutoff energy of 500eV in our following calculations; our calculated stable SFE γ_{I_2}

of pure Mg is about 33.85mJ/m^2, which is very close to the reported value by high precision

calculation methods.

A. Effect of strain on the SFEs and twinnability

　　We now study the effect of volumetric strain on the stable SFEs (γ_{I_2}, γ_{T_2}) and unstable

SFEs (γ_{UI_2}, γ_{UT_2}). Fig. 3 presents the variations of the stable and unstable SFEs of pure Mg

and Mg-Zn under volumetric strain, ranging from $\Delta V/V$=-0.12 to 0.13. It is shown that for all

four types of SFEs, the variations of SFEs with respect to the volumetric strain show strong similarity, *i.e.* the SFEs monotonically decrease with increasing $\Delta V/V$, but they remain positive. By multivariate regression analysis, the dependence of the stable and unstable SFEs on the volumetric stain can be well described by a polynomial fit $\gamma(mJ/m^2)=a+b(\Delta V/V)+c(\Delta V/V)^2+d(\Delta V/V)^3$ with the second derivative $d^2\gamma/d(\Delta V/V)^2>0$ (the fitting coefficients are provided in Table S1 in the Supplemental Material [36]). These observations indicate that volumetric compression has a greater influence on the SFE values than volumetric tension. It should be noted that a similar effect (*i.e.* cubic polynomial fit between the SFEs and volumetric strain) has also been reported for fcc copper [43], suggesting that this could be a generic volumetric strain effect, independent of crystal structure. In order to quantitatively account for the correlation between the applied strain and the resultant pressure, the hydrostatic pressure is calculated and shown in Fig. 3a and c. A continuous increase from -5.7GPa to 3.4GPa is observed for pure Mg, and from -5.3GPa to 3.6GPa for the Mg-Zn alloy, as $\Delta V/V$ increases from -0.12 to 0.13.

Using the calculated stable SFEs (γ_{I_2}, γ_{T_2}) and unstable SFEs (γ_{UI_2}, γ_{UT_2}), the twinnability of pure Mg and its alloys is characterized by the following ratio [6,8]:

$$\Lambda_{ratio}=\frac{\gamma_{UI_2}-\gamma_{I_2}}{\gamma_{UT_2}-\gamma_{I_2}}. \tag{7}$$

A larger value of Λ_{ratio} indicates a greater tendency towards the formation of twins. Fig. 3b and d present the change of Λ_{ratio} under volumetric strain. At equilibrium ($\Delta V/V$=0.00), it is seen that the Λ_{ratio} value of pure Mg (0.741) is larger than that of Mg-Zn alloy (0.678), but they are both much smaller than that of the Mg-Al alloy (0.800), indicating that the solute atom Al can promote twin formation, while the Zn atom decreases the potency to form a twin

in Mg-based alloy. As shown in the microstructures of the as-rolled Mg-1.5Zn and Mg-3Al at room temperature, Mg-3Al exhibits more extensive twinning as compared with Mg-1.5Zn [62], which indicates a greater tendency towards the formation of twins in Mg-Al alloys as compared with Mg-Zn alloy. This agrees well with our calculated result.

Under volumetric strain, the Λ_{ratio} increases rapidly from 0.708 to 0.788 for pure Mg, while for Mg-Zn, the Λ_{ratio} increases gradually from 0.678 to 0.686, as the strain $\Delta V/V$ changes from -0.12 to 0.13. These results indicate that a volumetric expansion promotes twin formation in pure Mg and Mg alloys. A similar trend of the effect of volumetric strain on SFEs and twinnability has also been observed in Mg-Al alloy; we refer to Fig. S2b in the Supplemental Material [36] for details.

B. Dislocation core structure and Peierls stress under strain

The dislocation core structure governs the dislocation mobility and ultimately the mechanical strength and ductility of materials. For instance, the planar core of dislocations in hcp and fcc metals determines their plastic flow propagation following the Schmid law, while the compact nonplanar core of bcc metals is known to be responsible for their violation of the Schmid law, exhibiting a tendency to three-way non-planar dissociation or polarization, implying a large Peierls stress that makes the screw dislocations difficult to move [63,64]. In addition, the core structure of misfit dislocations at heterostructure interfaces has also been found by MD simulations to play a critical role in determining dislocation nucleation and dissociation, transmission of lattice dislocations across the bimetal interface, and the interfacial sliding [65-67]. In terms of tuning the dislocation core structure, both experiments

and theoretical investigations [63] have shown that not only the impurities or alloying elements but also an application of external stresses can significantly alter the dislocation core structure and consequently its properties. However, although there have been some DFT studies of the Peierls barrier for various metals, they have been limited to zero-stress situations and do not provide information about the stress dependence of the Peierls potential. Therefore, in this section, we shall take Mg and Mg alloys as illustrations to show the significant strain effect on dislocation core structures and Peierls stresses.

We begin with the calculations of the dislocation core structure at equilibrium ($\Delta V/V$=0.00) by means of the semidiscrete variational PN model as described in Section 2. Fig. 2 presents the calculated dislocation core structures at equilibrium of pure Mg and Mg alloys with both edge and screw components; the calculated dislocation core structure parameters (d_x, d_z, w_x and w_z) at equilibrium are provided in Table 4, showing good agreement with previously reported experimental and theoretical values [17,68]. It is seen that the derived values of d_x/b are almost equal for pure Mg (7.50) and the Mg-Zn alloy (7.60), but they are much smaller than that of the Mg-Al alloy (9.74). Such a difference can be attributed to the lower value of the stable SFE γ_{I_2} for the Mg-Al alloy (22.50mJ/m^2) as compared to those for pure Mg (33.85mJ/m^2) and Mg-Zn alloy (31.64mJ/m^2) (see Table 3).

We next study the effect of strain on the dislocation core structure and the calculated results for pure Mg are presented in Fig. 4. The relevant key points are summarized below:

a) Under volumetric strain in dilatation or compression, the variation of d$_x$/b with respect to the strain follows a exponential function as $d_x/b=A\cdot\exp(\alpha\Delta V/V)$, where A=7.729 and α=4.49 (see Fig. 4a).

b) There are linear relationships between the calculated value of w_x/b and the applied volumetric strain with a proportional slope of $d(w_x/b)/d(\Delta V/V)=1.32$ (see Fig. 4b).

In an illustrative atomic-scale representation, Fig. 4c and d present the misfit densities and the pressure fields around dislocation cores [69] under various volumetric strains, respectively. As defined in Ref. [69], the pressure field around dislocation cores is expressed that

$$p(x,y)=-\frac{G(1+v)}{3\pi(1-v)}\sum_{i=1}^{2}\frac{b}{2}\cdot\frac{y+\text{sign}(y)w_e}{(x-d_{ei})^2+(y+\text{sign}(y)w_e)^2},\tag{8}$$

where $d_{e1}=d_x/2$, $d_{e2}=-d_x/2$, $w_e=w_x$, G is the shear modulus and v is the Poisson ratio. The atoms shown in Fig. 4d are color coded to distinguish the localized stress around the dislocation core. It is clearly seen that two partial dislocations (denoted by "⊥") are separated by a planar stacking fault in between. A large strain dependence is found for the dislocation core parameters, ranging from 4.82 to 16.67 for the stacking fault width d_x/b and from 0.41 to 0.77 for the partial core width w_x/b; these ranges are almost equal to those reported for 20 different Mg alloys at equilibrium (3.03 to 19.18 for d_x/b, and 0.55 to 0.72 for w_x/b [17]), indicating that strain has an even equally profound effect on the dislocation core structure with the chemical effect of solutes. Such results suggest potential foundations for the modification of strength and ductility of Mg and Mg-based alloys by strain engineering, *i.e.* preparing Mg alloys at different strain states. For instance, Yamashita *et al.* [70] verified experimentally that severe plastic deformation can improve the mechanical properties (e.g. strength and ductility) of Mg alloys. Therefore, it is expected that severe plastic deformation with specific constraint may provide an effective solution of strain engineering to improve

the mechanical properties of Mg alloys.

As described in Section 2.3 and illustrated in Fig. 5a, the Peierls stress is defined as the critical resolved shear stress for a dislocation moving through the lattice from one symmetrical configuration to another equivalent symmetrical configuration [56,57,71]. Fig. 5b presents our calculated dependence of the Peierls stresses of pure Mg and Mg alloys under volumetric strain. The logarithm of the Peierls stress $\ln(\tau_p)$ of pure Mg and Mg alloys shows a linearly decreasing trend with increasing strain, following a slope of $d(\ln(\tau_p))/d(\Delta V/V)=$ -18.74 for pure Mg. Therefore, the Peierls stress τ_p can be approximated as an exponential relationship with the volumetric strain, and a general conclusion can be drawn for the strain effect on Peierls stress such that a compressive strain leads to a strain strengthening effect, while a tensile strain causes strain softening.

Under volumetric compression, the Peierls stress of the dislocation lying in the basal plane increases, which may eventually promote the activation of non-basal slip systems and consequently ductilize Mg and Mg alloys. These conclusions agree well with the experimental observations that the non-basal slip systems can be activated by hydrostatic pressure [24-26]. Although the strain effect on the Peierls stress is found to be far more profound than the chemical effect of solutes by the analysis of data published in Ref. [17], we would like to emphasize that both the strain strengthening and solute strengthening play important and potentially complementary roles in strengthening and ductilizing Mg alloys, since the solute atoms may provide an additional "pinning" effect due to the solute/dislocation interactions [18].

C. Electronic origin of the strain effects

Based on previous studies [8-12], it is believed that the charge density distributions could provide a physical explanation for the SFEs of pure Mg and Mg alloys. To clarify the strain effect on the polarization and charge transfer, we have calculated the valence charge density difference (VCDD) which is defined as:

$$\Delta\rho(Mg_{47}X) = \rho_{sc}(Mg_{47}X) - \rho_{nsc}(Mg_{47}X), \tag{9}$$

where $\rho_{sc}(Mg_{47}X)$ is the charge density after reaching electronic self-consistency and $\rho_{nsc}(Mg_{47}X)$ is the charge density prior to electronic self-consistent calculation, *i.e.* representing a summation of atomic charge densities (or the non-interacting charge density). Fig. 6 (a-c) illustrates the VCDDs of pure Mg under different volumetric strains. It is seen that the charge density decreases with the increasing volumetric strain at hollow sites (indicated by the red dashed circle in Fig. 6) which may provide a basis for the effect of strain on SFEs, as the denser VCDD produces a stronger bonding of Mg-Mg [8].

To underline the strain effect of Mg alloys, Fig. 6 also presents the calculated VCDDs of Mg-Zn (Fig S3 for Mg-Al in the Supplemental Material [36]) under different volumetric strains. It can be seen that under the volumetric strain, the VCDD decreases with increasing strain for both Mg-Zn and Mg-Al alloys at hollow sites, producing a same effect on the Mg alloys as on pure Mg. Comparing the VCDDs of pure Mg and Mg alloys at the unstrained state ($\Delta V/V$=0.00), it is found that Zn and Al solute atoms decrease the VCDD at the circled region in red, being responsible for the lower value of SFEs for the Mg-Zn and Mg-Al alloys as compared to those of pure Mg (see Table 3). By comparing the chemical effect of solute and the strain effect on the VCDD, it can be concluded that the chemical effect may

effectively change the shapes of VCDD isosurface, while the strain effect will enhance the magnitude of the isosurface, indicating a general rule that a higher SFE corresponds to more profound electronic polarization induced by compressive strain.

IV. DISCUSSION

In general, the solute strengthening provides an effective strengthening pathway for the development of novel Mg alloys which can potentially resolve the trade-off dilemma between strength and ductility and the poor workability and formability. In Mg alloys, solute atoms can disturb the charge density ("chemical factor") and produce a local strain field ("strain factor") due to the different atomic radii between Mg and solute atoms, which are two supposed reasons for the solute effect on the SFEs. The local strain caused by solute atoms is equivalent to the external strain by changing the lattice geometry. For example, Liu *et al.* [12] found that the activation of slip systems is closely related to the change of the local ratio of *c/a* by different solute elements, being responsible for the solute strengthening and/or ductilizing. Shang *et al.* [8] has recently found an approximate linear relationship between the SFEs and the equilibrium volumes of Mg alloys by different alloying elements, which raises an interesting question whether the change of SFEs can be partially attributed to the strain effect. Our results, that a local compressive strain will promote larger SFEs whereas lattice dilatation will generate smaller SFEs, provide a novel view on the contribution to SFEs by solute introduction.

Although the study of the strain effect on the SFEs could offer insights into the "strain factor" of the solute effect on the SFEs and the mechanism of solute strengthening as the size

misfit in the model of solute strengthening [18,69,72], thus far however, the effect of an external strain is absolutely ignored. As seen in the preceding sections, an external strain plays an important role on the SFEs and dislocation core structures. The strain effect cannot be ignored in experimentally achievable strains such as under high pressure, in high strain rate deformation, shock loading [73] and severe plastic deformation (SPD) processing. For example, the effect of super-high pressure on the mechanical properties of Mg alloys has been studied experimentally, with a maximum pressure of 6GPa [31,32]. At such high strain, the SFEs can change by ~40% relative to those at zero-strain, which consequently produces an ~340% increase of Peierls stress from 8.4MPa to 36.7MPa, and ~30% variation of dislocation core structure.

As shown in Fig. 7a, a strong inverse relationship between the d_x/b and the stable SFE γ_{I_2} is found for Mg and Mg alloys. It is, however, not a simple linear relationship as proposed for fcc metals in Ref. [74,75] using a DFT-informed PFDD model. The correlation fits well with the exponential function as

$$d_x/b = A \cdot \exp(-\alpha\gamma_{I_2}) + B \cdot \exp(-\beta\gamma_{I_2}),\qquad(10)$$

where A=23.92, B=0.09051, α=-0.03841 and β=0.05522. Meanwhile an inverse linear relationship between the logarithm of the Peierls stress $\ln(\tau_p)$ and the dislocation width (w_x/b) (Fig. 7b) is obtained by fitting the formula

$$\ln(\tau_P) = Aw_x/b + B,\qquad(11)$$

where A=-13.73 and B=9.031. This provides a variant of the well-known formula $\tau_p = A\exp(-\alpha\xi/b)$ [56], where A and α are constants and ξ is the dislocation half-width and approximatively equal to the w_x in Eq. (11). Furthermore, the value of w_x/b is found to

have a strong correlation with the unstable SFE γ_{UI_2} (Fig. 7c), and the fitting function for Mg and Mg alloys is generally expressed as

$$w_x/b=A\cdot\exp(-\alpha\gamma_{UI_2}), \tag{12}$$

where A=1.24 and α=-0.00921. This logarithm of the Peierls stress $\ln(\tau_p)$ can also show an exponential correlation with the unstable SFE γ_{UI_2} (Fig. 7d), and the formula is obtained as

$$\ln(\tau_P)=A\cdot\exp(-\alpha\gamma_{UI_2})+B, \tag{13}$$

where A=-17.03, B=9.031 and α=-0.00921. With these relationships, one may simply predict the Peierls stress of Mg alloys even under strain. It is generally accepted that Mg alloys with high basal and low non-basal unstable SFEs will have higher both strength and ductility than those of pure Mg, because the high and low Peierls stresses on the basal plane and on non-basal planes, respectively, will benefit the activation of non-basal slip system, aiding both strengthening and ductilizing of Mg alloys.

In summary, the effect of strain on the SFEs, dislocation core structure and Peierls stress can be particularly important for understanding the mechanical behavior of metals in high pressure experiments, severe plastic deformation and shock-loading conditions [73]. Therefore, our results may provide an additional contribution and pathway to solve the tradeoff between strength and ductility based on the dependence of SFEs on external parameters such as strain.

V. CONCLUSIONS

We have performed comprehensive investigations on the effect of volumetric strain on the SFEs, dislocation core structure and Peierls stress of Mg and Mg alloys based on DFT

calculations and the semidiscrete variational PN model. The results are summarized as follows:

(1) Strain can affect the values of SFEs, making them either larger or smaller, and thus changing the twinnabilities of pure Mg and Mg alloys. The SFEs and twinnability of Mg-Zn and Mg-Al alloys will be changed by volumetric strain in a similar manner to pure Mg.

(2) In general, a narrow (wide) dislocation core will decrease (increase) the mobility of dislocation. The dislocation core structure and Peierls stress may be significantly modified by strains as the variation of SFEs, which could promote the activation or operation of non-basal slip system, in agreement with experimental results.

(3) Besides of external strain, the strain may also be imposed by the introduction of solute atoms in experiments, therefore the strain effect on the SFEs found in the present study may provide a novel view on the "strain factor" of the solute effect by the introduction of local strain fields that was assumed based on experimental observations.

(4) General exponential relationships are proposed between the dislocation core structure, the Peierls stress and the stable or unstable SFEs, which provides a foundation for further experiments. For instance, the separation distance between two partials shows a universal exponential relationship with the stable SFE γ_{I_2}, while the Peierls stress is exponentially dependent on the unstable SFE γ_{UI_2}.

ACKNOWLEDGEMENTS

REFERENCES

[1] J. Hirsch and T. Al-Samman, Acta Mater. **61**, 818 (2013).

[2] H. Furuya, N. Kogiso, S. Matunaga, and K. Senda, in *Mater. Sci. Forum* (Trans Tech Publ, 2000), pp. 341.

[3] E. Schubert, M. Klassen, I. Zerner, C. Walz, and G. Sepold, J. Mater. Process. Technol. **115**, 2 (2001).

[4] Q. Z. Chen and G. A. Thouas, Mater. Sci. Eng. R-Rep. **87**, 1 (2015).

[5] R. Verma, L. G. Hector, P. E. Krajewski, and E. M. Taleff, JOM **61**, 29 (2009).

[6] J. Han, X. M. Su, Z. H. Jin, and Y. T. Zhu, Scr. Mater. **64**, 693 (2011).

[7] M. Muzyk, Z. Pakiela, and K. J. Kurzydlowski, Scr. Mater. **66**, 219 (2012).

[8] S. L. Shang, W. Y. Wang, B. C. Zhou, Y. Wang, K. A. Darling, L. J. Kecskes, S. N. Mathaudhu, and Z. K. Liu, Acta Mater. **67**, 168 (2014).

[9] W. Y. Wang, S. L. Shang, Y. Wang, Z. G. Mei, K. A. Darling, L. J. Kecskes, S. N. Mathaudhu, X. D. Hui, and Z. K. Liu, Mater. Res. Lett. **2**, 29 (2014).

[10] Y. F. Wu, S. Li, Z. G. Ding, W. Liu, Y. H. Zhao, and Y. T. Zhu, Scr. Mater. **112**, 101 (2016).

[11] Q. Zhang, L. Fu, T. W. Fan, B. Y. Tang, L. M. Peng, and W. J. Ding, Physica B **416**, 39 (2013).

[12] Z. R. Liu and D. Y. Li, Acta Mater. **89**, 225 (2015).

[13] J. A. Yasi, L. G. Hector, and D. R. Trinkle, Acta Mater. **60**, 2350 (2012).

[14] M. H. Yoo, Metall. Trans. A **12**, 409 (1981).

[15] J. Y. Min, L. G. Hector, J. P. Lin, J. T. Carter, and A. K. Sachdev, Int. J. Plast **57**, 52

(2014).

[16] S. Sandlöbes, Z. R. Pei, M. Friák, L. F. Zhu, F. Wang, S. Zaefferer, D. Raabe, and J. Neugebauer, Acta Mater. **70**, 92 (2014).

[17] Z. R. Pei, D. C. Ma, M. Friák, B. Svendsen, D. Raabe, and J. Neugebauer, Phys. Rev. B **92**, 064107 (2015).

[18] J. A. Yasi, L. G. Hector, and D. R. Trinkle, Acta Mater. **58**, 5704 (2010).

[19] J. A. Yasi, L. G. Hector, and D. R. Trinkle, Acta Mater. **59**, 5652 (2011).

[20] M. Ghazisaeidi, L. G. Hector, and W. A. Curtin, Acta Mater. **80**, 278 (2014).

[21] G. P. M. Leyson, L. G. Hector, and W. A. Curtin, Acta Mater. **60**, 5197 (2012).

[22] T. W. Fan, L. G. Luo, L. Ma, B. Y. Tang, L. M. Peng, and W. J. Ding, Mater. Sci. Eng. A-Struct. Mater. Prop. Microstruct. Process. **582**, 299 (2013).

[23] A. Moitra, S. G. Kim, and M. F. Horstemeyer, Acta Mater. **75**, 106 (2014).

[24] F. Kang, Z. Li, J. T. Wang, P. Cheng, and H. Y. Wu, J. Mater. Sci. **47**, 7854 (2012).

[25] F. Kang, J. Q. Liu, J. T. Wang, X. Zhao, X. L. Wu, and K. N. Xia, Int. J. Mater. Res. **100**, 1686 (2009).

[26] F. Kang, J. Q. Liu, J. T. Wang, and X. Zhao, Scr. Mater. **61**, 844 (2009).

[27] E. Lilleodden, Scr. Mater. **62**, 532 (2010).

[28] Y. N. Wang and J. C. Huang, Acta Mater. **55**, 897 (2007).

[29] J. C. F. Millett, S. M. Stirk, N. K. Bourne, and G. T. Gray, Acta Mater. **58**, 5675 (2010).

[30] P. J. Hazell, G. J. Appleby-Thomas, E. Wielewski, C. Stennett, and C. Siviour, Acta Mater. **60**, 6042 (2012).

[31] S. Zhao, Q. Peng, H. Li, and B. Liu, J. Alloys Compd. **584**, 56 (2014).

[32] H. Fu, N. Liu, Z. Zhang, and Q. Peng, Journal of Magnesium and Alloys **4**, 302 (2016).

[33] G. Kresse and J. Furthmüller, Phys. Rev. B **54**, 11169 (1996).

[34] G. Kresse and D. Joubert, Phys. Rev. B **59**, 1758 (1999).

[35] J. P. Perdew, K. Burke, and M. Ernzerhof, Phys. Rev. Lett. **77**, 3865 (1996).

[36] See Supplemental Material at [URL will be inserted by publisher] for details of the fitting coefficients of the cubic polynomial fit, the convergence of the stable SFE as a function of k-mesh grid as well as the SFEs and VCDDs of Mg-Al alloy under the volumetric strains.

[37] M. Methfessel and A. T. Paxton, Phys. Rev. B **40**, 3616 (1989).

[38] F. W. Von Batchelder and R. F. Raeuchle, Phys. Rev. **105**, 59 (1957).

[39] L. G. Hector Jr, J. F. Herbst, W. Wolf, P. Saxe, and G. Kresse, Phys. Rev. B **76**, 014121 (2007).

[40] C. Wang, H. Y. Wang, T. L. Huang, X. N. Xue, F. Qiu, and Q. C. Jiang, Sci. Rep. **5** (2015).

[41] E. Clouet, Phys. Rev. B **86**, 144104 (2012).

[42] M. Jahnátek, J. Hafner, and M. Krajci, Phys. Rev. B **79**, 224103 (2009).

[43] P. S. Branicio, J. Y. Zhang, and D. J. Srolovitz, Phys. Rev. B **88**, 064104 (2013).

[44] J. A. Yasi, T. Nogaret, D. R. Trinkle, Y. Qi, L. G. Hector Jr, and W. A. Curtin, Modell. Simul. Mater. Sci. Eng. **17**, 055012 (2009).

[45] M. Ghazisaeidi, L. G. Hector, and W. A. Curtin, Scr. Mater. **75**, 42 (2014).

[46] C. Woodward, D. R. Trinkle, L. G. Hector Jr, and D. L. Olmsted, Phys. Rev. Lett. **100**, 045507 (2008).

[47] S. K. Yadav, R. Ramprasad, A. Misra, and X. Y. Liu, Acta Mater. **74**, 268 (2014).

[48] V. V. Bulatov and E. Kaxiras, Phys. Rev. Lett. **78**, 4221 (1997).

[49] G. Lu, in *Handbook of Materials Modeling* (Springer, 2005), pp. 793.

[50] G. Schoeck, Philos. Mag. A **69**, 1085 (1994).

[51] G. Schoeck, Philos. Mag. A **81**, 1161 (2001).

[52] A. R. Wazzan and L. B. Robinson, Phys. Rev. **155**, 586 (1967).

[53] V. Bulatov and W. Cai, *Computer simulations of dislocations* (Oxford University Press on Demand, 2006), Vol. 3.

[54] R. Poli, Journal of Artificial Evolution and Applications **2008**, 3 (2008).

[55] J. Kennedy, in *Encyclopedia of machine learning* (Springer, 2011), pp. 760.

[56] B. Joos and M. S. Duesbery, Phys. Rev. Lett. **78**, 266 (1997).

[57] P. Cordier, J. Amodeo, and P. Carrez, Nature **481**, 177 (2012).

[58] Q. Zhang, T. W. Fan, L. Fu, B. Y. Tang, L. M. Peng, and W. J. Ding, Intermetallics **29**, 21 (2012).

[59] J. Zhang, Y. C. Dou, G. B. Liu, and Z. X. Guo, Comput. Mater. Sci. **79**, 564 (2013).

[60] X. Z. Wu, R. Wang, and S. F. Wang, Appl. Surf. Sci. **256**, 3409 (2010).

[61] X. Y. Cui, H. W. Yen, S. Q. Zhu, R. K. Zheng, and S. P. Ringer, J. Alloys Compd. **620**, 38 (2015).

[62] Y. Chino, T. Ueda, Y. Otomatsu, K. Sassa, X. S. Huang, K. Suzuki, and M. Mabuchi, Mater. Trans. **52**, 1477 (2011).

[63] D. Weygand, M. Mrovec, T. Hochrainer, and P. Gumbsch, Ann. Rev. Mater. Res. **45**, 369 (2015).

[64] E. Clouet, D. Caillard, N. Chaari, F. Onimus, and D. Rodney, Nat. Mater. **14**, 931 (2015).

[65] R. F. Zhang, I. J. Beyerlein, S. J. Zheng, S. H. Zhang, A. Stukowski, and T. C. Germann, Acta Mater. **113**, 194 (2016).

[66] R. F. Zhang, T. C. Germann, X. Y. Liu, J. Wang, and I. J. Beyerlein, Acta Mater. **79**, 74 (2014).

[67] R. F. Zhang, J. Wang, I. J. Beyerlein, A. Misra, and T. C. Germann, Acta Mater. **60**, 2855 (2012).

[68] J. N. Wang, Mater. Sci. Eng. A-Struct. Mater. Prop. Microstruct. Process. **206**, 259 (1996).

[69] D. Ma, M. Friák, J. von Pezold, D. Raabe, and J. Neugebauer, Acta Mater. **85**, 53 (2015).

[70] A. Yamashita, Z. Horita, and T. G. Langdon, Mater. Sci. Eng. A-Struct. Mater. Prop. Microstruct. Process. **300**, 142 (2001).

[71] F. R. N. Nabarro, Mater. Sci. Eng. A-Struct. Mater. Prop. Microstruct. Process. **234**, 67 (1997).

[72] G. P. M. Leyson, L. G. Hector, and W. A. Curtin, Acta Mater. **60**, 3873 (2012).

[73] R. F. Zhang, T. C. Germann, J. Wang, X. Y. Liu, and I. J. Beyerlein, Scr. Mater. **68**, 114 (2013).

[74] A. Hunter, R. F. Zhang, I. J. Beyerlein, T. C. Germann, and M. Koslowski, Modell. Simul. Mater. Sci. Eng. **21**, 025015 (2013).

[75] A. Hunter, R. F. Zhang, and I. J. Beyerlein, J. Appl. Phys. **115**, 134314 (2014).

TABLES

TABLE 1. The calculated lattice constants *a* and *c* (in Angstroms) and cohesive energy E_c

(eV/atom) of pure Mg together with other theoretical values [38-40].

	Refs.	Lattice constants		E_c
		a	*c*	
pure Mg	This work	3.195	5.172	-1.50
	Exp. [38]	3.21[a]	5.21[a]	
	Cal. [40]	3.221	5.178	-1.44
	Cal. [39]	3.19	5.17	

[a] These experimental values are acquired at 298K.

TABLE 2. The calculated elastic constants c_{ij}, the derived Hill average bulk moduli B_H, shear moduli G_H and Young's moduli E_H (all in GPa), and the Poisson ratio v_H of pure Mg, which are the input parameters for the semidiscrete variational PN model, together with the experimental data and other theoretical values [40,52].

Material	c_{11}	c_{12}	c_{13}	c_{33}	c_{44}	B_H	G_H	E_H	v_H	K_e	K_s
hcp Mg[a]	69.12	21.84	20.01	70.84	16.37	36.98	20.70	52.34	0.264	2.238	1.647
hcp Mg[b]	59.5	26.12	21.8	61.55	16.35	35.55	17.21	44.45	0.292	1.934	1.370
hcp Mg[c]	63.1	22.2	22.7	66.3	22.6	36.4	21.5	53.8	0.254	2.293	1.711

[a] This work.

[b] Exp. [52], and these experimental values are acquired at 298K.

[c] Cal. [40].

TABLE 3. The calculated stable SFEs (γ_{I_2}, γ_{T_2}) and unstable SFEs (γ_{UI_2}, γ_{UT_2}) of pure Mg and Mg alloys together with previous theoretical values (in mJ/m^2). x_g (%) and x_{SF} (%) are the global solute concentration and the areal concentration within the stacking fault plane, respectively.

Mg-X	x_g	x_{SF}	γ_{I_2}	γ_{UI_2}	γ_{T_2}	γ_{UT_2}	NOTE
Mg			33.85	93.57	41.36	114.46	This work，alias shear, GGA-PBE
			20.1	95.8	38.2	120.3	CASTEP, slab shear, GGA-PW91 [40]
			26.1	94.9	37.1	111.2	VASP, alias shear, GGA-PBE [8]
			36	92	39	111	VASP, slab shear, GGA-PBE [7]
			30.0		40.0		VASP, alias shear, GGA-PBE [10]
			29.1				ANNNI framework [12]
			33		42		VASP, CINEB [6]
			33.8	87.6			VASP, slab shear, GGA-PW91[11]
			21.4				VASP, slab shear, GGA-PBE[59]
			21	88			VASP, slab shear, GGA-PW91[60]
			33.8	87.6	40.2	154.3	VASP, slab shear, GGA-PW91 [58]
			48.2				VASP, slab shear [9]
			35.4				VASP, slab shear [61]
Al	2.08	25	22.50	87.62	38.01	108.26	This work, alias shear, GGA-PBE
	1.04	8.33	24.8		36.0		VASP, alias shear, GGA-PBE [8]
	2.08	25	21		32		VASP, slab shear, GGA-PBE [7]
	0.69	8.33	29.7		37.1		VASP, alias shear, GGA-PBE [10]
	1.67	50	23		42		VASP, CINEB [6]
	0.78	6.25	33.6				VASP, slab shear [9]
Zn	2.08	25	31.64	85.43	39.77	106.43	This work, alias shear, GGA-PBE
	1.04	8.33	25.5		37.2		VASP, alias shear, GGA-PBE [8]
	2.08	25	37		43		VASP, slab shear, GGA-PBE [7]
	0.69	8.33	26.2		37.6		VASP, alias shear, GGA-PBE [10]
	0.93	11.11	35.1	94.2			VASP, slab shear, GGA-PW91[11]
	0.78	6.25	30.8				VASP, slab shear [9]
	2.08	25	35				VASP, alias shear [17]

TABLE 4. The geometrical parameters of dislocation core structure and the calculated Peierls stress (τ_p) in MPa of pure Mg and Mg alloys together with other predictions from the literatures at equilibrium (with $\Delta V/V$=0.00).

Solute	d_x/b	w_x/b	d_z/b	w_z/b	τ_p	NOTE
Mg	7.50	0.54	7.56	0.58	8.40	This work, DFT
	7.00	0.68	7.18	0.60	1.15	Ref. [17] DFT
					6.73[a]	Exp. [68]
	3.06	0.45	2.90	0.38	22.9	Ref. [17] EAM
Al	9.74	0.54	9.79	0.58	3.94	This work, DFT
Zn	7.60	0.56	7.65	0.62	2.61	This work, DFT
	6.94	0.64	7.11	0.52	2.53	Ref. [17] DFT

[a] This experimental value is based on yield stress data at 0K.

FIGURES

FIG. 1. (Color online) (a) Schematic illustration of the perfect lattice, basal stacking fault I_2, and twin stacking fault T_2 configurations generated via the alias shear. The letters A, B and C represent different stacking sequences of (0001) planes, which are identified by blue, pink and olive symbols respectively, with the stacking fault being highlighted in red. The solid and open circles represent the atomic coordinates at 0 and ½ along $[11\overline{2}0]$ direction, respectively, and the dotted line indicates the stacking fault position. (b) The full γ surface of pure Mg for the basal (0001) plane. (c) The calculated SFE profiles of pure Mg, Mg-Al and Mg-Zn along the $[11\overline{2}0]$ direction to indicate the stable SFEs (γ_{I_2} and γ_{T_2}) and unstable SFEs (γ_{UI_2} and γ_{UT_2}).
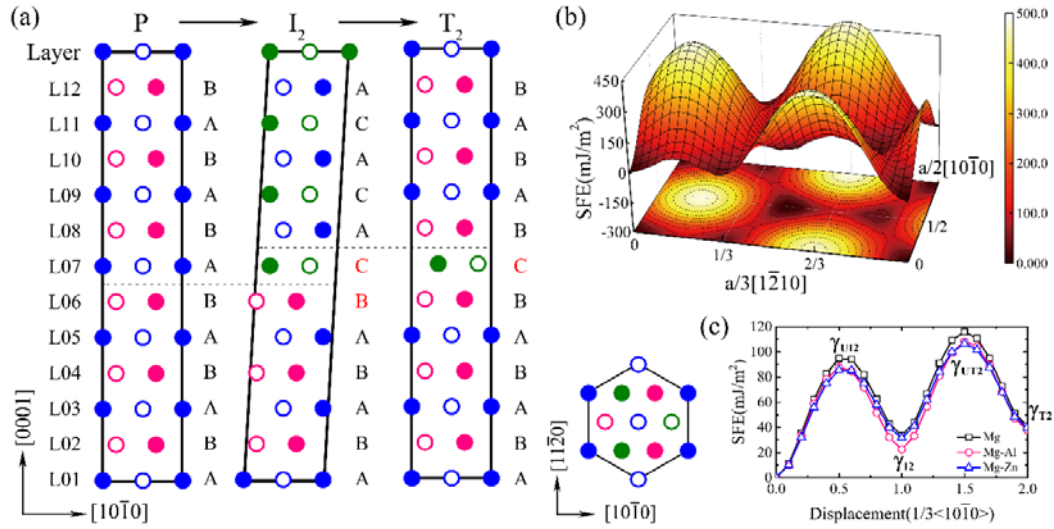
FIG. 2. (Color online) (a) A schematic to illustrate the dissociation of a perfect dislocation into two partials. The $\vec{b}_1$, $\vec{b}_2$ and $\vec{b}_3$ are the Burgers vectors of perfect dislocation and the $\vec{b}_{p1}$, $\vec{b}_{p2}$ and $\vec{b}_{p3}$ are the Burgers vectors of partial dislocation. The $\vec{b}_{p3,x}$, $\vec{b}_{p3,z}$, $\vec{b}_{-p1,x}$ and $\vec{b}_{-p1,z}$ are the components of $\vec{b}_{p3}$ and $\vec{b}_{-p1}$ along x and z-axes, respectively. (b-f) The dislocation core structure of pure Mg (black curve) and Mg alloys (pink curve for the Mg-Al alloy and blue curve for the Mg-Zn alloy) at equilibrium. The separation d_x (or d_z) between the edge (or screw) components of the two partials is defined as the distance between the two peaks, and the width w_x (or w_z) of the edge (or screw) components of a partial dislocation is the full width at half maximum approximately, as shown in this figure.
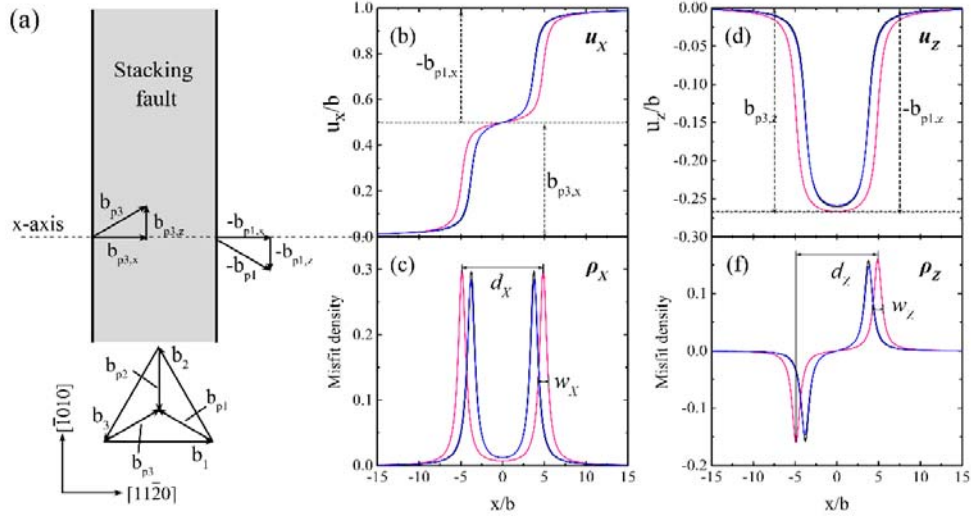
FIG. 3. (Color online) The calculated stable and unstable SFEs, the pressure, and the twinnability for (a-b) pure Mg and (c-d) Mg-Zn as a function of volumetric strain. It is found that the dependence of the stable and unstable SFEs on the volumetric stain can be well described by a polynomial fit.
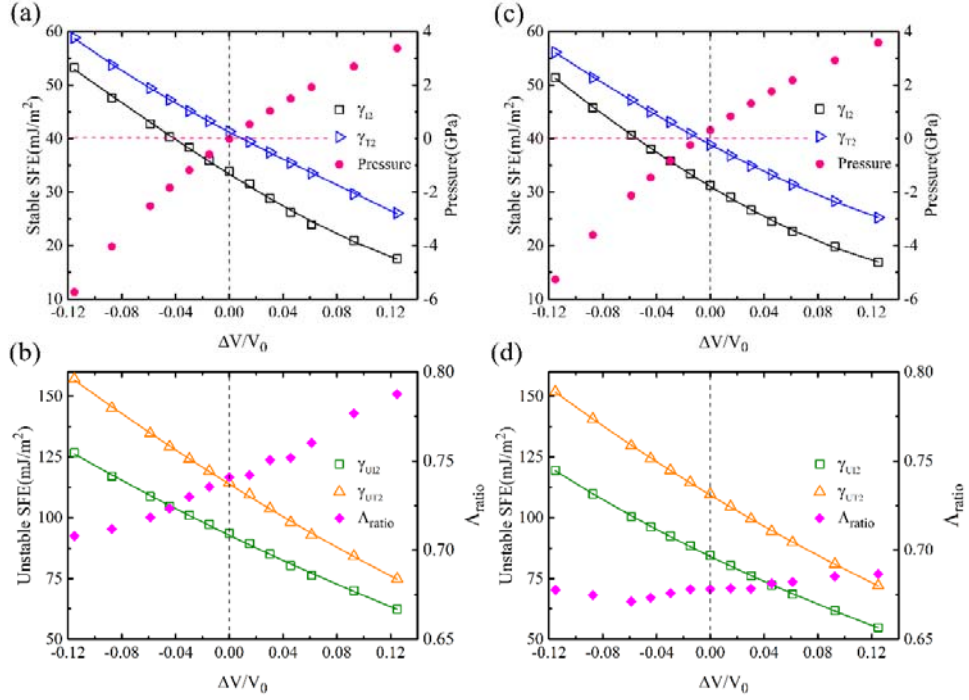
FIG. 4. (Color online) The (a) distance (d_x/b) and (b) width (w_x/b) between the edge components of a dislocation under different volumetric strains. (c) The misfit density and (d) the pressure field (in GPa) produced by the dislocation under different volumetric strains. It is seen that, under volumetric strain in dilatation or compression, the variation of d_x/b with respect to the strain follows the exponential function, while the calculated value of w_x/b is linearly dependent on the applied volumetric strain.
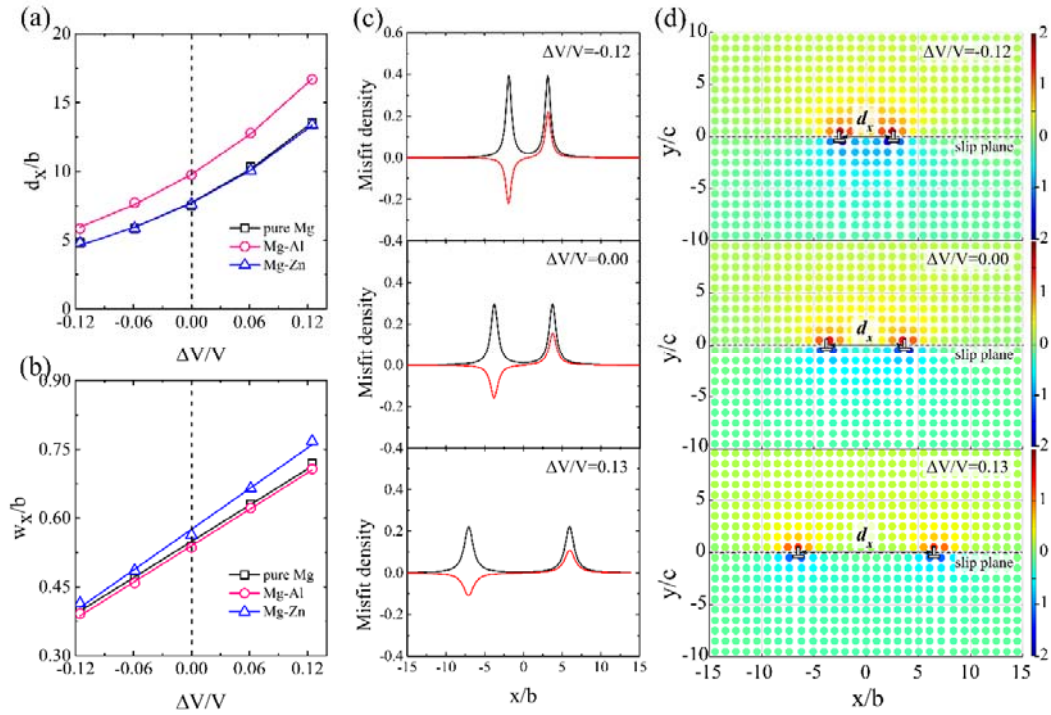
FIG. 5. (Color online) (a) A schematic to represent the dislocation movement from one symmetrical configuration to another equivalent symmetrical configuration. (b) The logarithm of Peierls stress under different volumetric strains for pure Mg and Mg alloys, which shows a linearly decreasing trend with increasing strain.
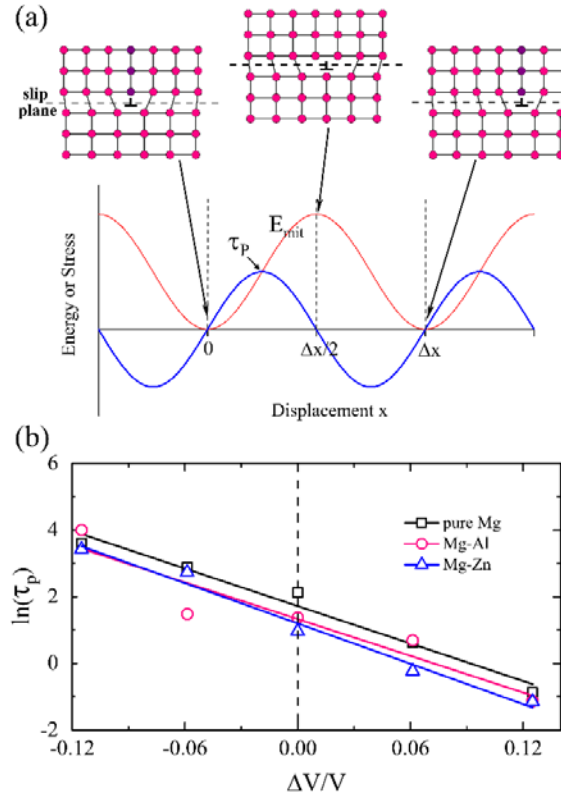
FIG. 6. (Color online) Contour plots of the valence charge density difference (VCDD) of pure Mg and Mg-Zn alloy under the volumetric strains: (a, d) $\Delta V/V$=-0.12, (b, e) $\Delta V/V$=0.00 and (c, f) $\Delta V/V$=0.13 respectively. The unit of VCDD is electrons/Bohr^3, and the thin black line corresponds to the isosurface of 0.0018electrons/Bohr^3. It is illustrated that the charge density decreases with the increasing volumetric strain at hollow sites (indicated by the red dashed circles).
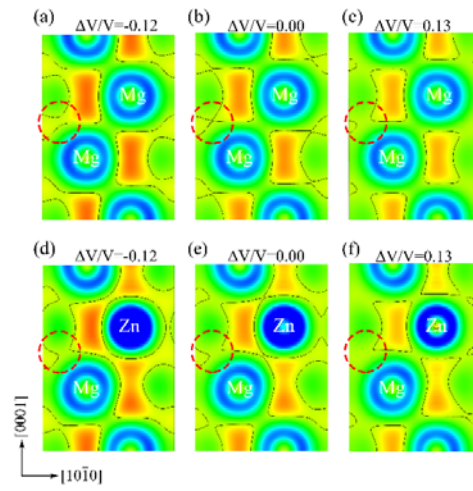
FIG. 7. (Color online) The relationship between the dislocation core structure, the Peierls stress and the SFEs. The black, pink and blue points correspond to pure Mg, Mg-Al alloy and Mg-Zn alloy, respectively, and the red solid lines are calculated by the relationships Eq. (10)-(13), indicating that there are general exponential relationships between the dislocation core structure, the Peierls stress and the stable or unstable SFEs.